Phosphorylated filamin A regulates actin-linked caveolae dynamics

Olivia Muriel[1], Asier Echarri[1], Christian Hellriegel[2], Dácil M. Pavón[1], Leonardo Beccari[3] and Miguel A. Del Pozo[1,*]

[1]Integrin Signaling Laboratory, Department of Vascular Biology, Centro Nacional de Investigaciones Cardiovasculares (CNIC), Melchor Fernández Almagro 3, 28029 Madrid, Spain
[2]Microscopy and Dynamic Imaging Unit, Centro Nacional de Investigaciones Cardiovasculares (CNIC), Melchor Fernández Almagro 3, 28029 Madrid, Spain
[3]Morphogenesis and differentiation of the vertebrate CNS. Centro de Biología Molecular 'Severo Ochoa', Consejo Superior de Investigaciones Científicas (CSIC)-Universidad Autónoma de Madrid, Nicolás Cabrera 1, 28049 Madrid, Spain
*Author for correspondence (madelpozo@cnic.es)

Accepted 20 April 2011
Journal of Cell Science 124, 2763-2776

doi:10.1242/jcs.080804

Summary

Caveolae are relatively stable membrane invaginations that compartmentalize signaling, regulate lipid metabolism and mediate viral entry. Caveolae are closely associated with actin fibers and internalize in response to diverse stimuli. Loss of cell adhesion is known to induce rapid and robust caveolae internalization and trafficking toward a Rab11-positive recycling endosome; however, pathways governing this process are poorly understood. Here, we report that filamin A is required to maintain the F-actin-dependent linear distribution of caveolin-1. High spatiotemporal resolution particle tracking of caveolin-1–GFP vesicles by total internal reflection fluorescence (TIRF) microscopy revealed that FLNa is required for the F-actin-dependent arrest of caveolin-1 vesicles in a confined area and their stable anchorage to the plasma membrane. The linear distribution and anchorage of caveolin-1 vesicles are both required for proper caveolin-1 inwards trafficking. De-adhesion-triggered caveolae inward trafficking towards a recycling endosome is impaired in FLNa-depleted HeLa and FLNa-deficient M2-melanoma cells. Inwards trafficking of caveolin-1 requires both the ability of FLNa to bind actin and cycling PKCα-dependent phosphorylation of FLNa on Ser2152 after cell detachment.

Key words: Trafficking, Actin cytoskeleton, Cell adhesion, Signaling, filamin A, caveolin-1, Vesicle tracking

Introduction

Caveolae are sphingolipid- and cholesterol-enriched plasma membrane (PM) invaginations (Parton and Simons, 2007) that modulate multiple signaling pathways by regulating the trafficking of membrane receptors, tyrosine kinases and small Rho GTPases (del Pozo et al., 2005; Grande-Garcia et al., 2007; Parton and Simons, 2007). Caveolae also mediate the entry of lipoproteins, thus modulating lipid metabolism (Fernandez-Hernando et al., 2009). Caveolae can undergo endocytosis under certain circumstances (Parton and Simons, 2007), including upon SV40 infection (Pelkmans et al., 2001), lipid modification (Sharma et al., 2004), hyperosmotic and heat shock (Kang et al., 2000; Parton et al., 1994), mitosis (Boucrot et al., 2011) and integrin-mediated loss of adhesion to the extracellular matrix (ECM) (del Pozo et al., 2004). Integrin-mediated loss of adhesion is physiologically relevant in events, such as mitosis and directional cell migration, where the cell detaches from the ECM in localized areas. By mediating caveolae internalization, caveolin-1 (Cav1) regulates Rac1 PM targeting, and hence directs cell migration (Grande-Garcia et al., 2007) and controls cell proliferation and anchorage-independent growth (Cerezo et al., 2009). Cell detachment also occurs during intravascular tumoral dissemination towards metastatic foci. Cav1 vesicles also undergo microtubule-dependent long-range movement towards an internal compartment (Mundy et al., 2002; McMahon et al., 2009) and a specialized type of movement at the basal PM called kiss-and-run (Pelkmans and Zerial, 2005). Internalization of caveolae and resident proteins is crucial for the regulation of multiple signal transduction pathways (Anderson, 1993; Parton and Simons, 2007). Proteins shown to regulate caveolae internalization include Src (Shajahan et al., 2004), protein kinase C (PKC) α (Smart et al., 1995) and intersectin (Predescu et al., 2003).

Caveolae biology is intimately linked to the actin cytoskeleton (Kanzaki and Pessin, 2002; Richter et al., 2008; Rothberg et al., 1992; Stahlhut and van Deurs, 2000), which is a key regulator of caveolae endocytosis (Mundy et al., 2002; Parton et al., 1994). Caveolae are thought to be physically linked to actin fibers (Richter et al., 2008; Stahlhut and van Deurs, 2000), but linker proteins between these structures have not been identified.

Some of the most prominent actin-crosslinking proteins are the filamins. Among the three filamin isoforms in humans, filamin A (FLNa) is the most widely expressed and abundant. FLNa forms dimers that associate at their C-terminus and contains an N-terminal actin-binding domain (Stossel et al., 2001). FLNa is reported to be the most potent actin-filament crosslinking protein that is able to construct orthogonal actin networks in vitro (Bennett et al., 1984; Brotschi et al., 1978; Stossel et al., 2001). Several studies have shown that FLNa is required for maintenance of PM stability and for proper locomotion in FLNa-deficient M2-melanoma cells (Cunningham et al., 1992) and for the generation of broad surface protrusions necessary for locomotion and phagocytosis in *Dictyostelium* (Cox et al., 1996). FLNa associates with lipid membranes (Isenberg, 1991; Isenberg and Niggli, 1998) and binds to several receptors at the cell surface, such as β-integrins (Stossel

et al., 2001). Through its C-terminus, FLNa binds multiple proteins, including PKCα, which localizes in caveolae (Smart et al., 1995), and several Ras superfamily GTPases.

FLNa function is regulated by phosphorylation at the conserved consensus phosphorylation site Ser2152 (van der Flier and Sonnenberg, 2001). Several kinases phosphorylate Ser2152, including PAK1 (Vadlamudi et al., 2002), PKA (Jay et al., 2004), Akt (Ravid et al., 2008) and ribosomal protein S6 kinase α-3 (p90 RSK2) (Woo et al., 2004). Ca^{2+}/calmodulin-dependent protein kinase type II (CaMK-II) (Ohta and Hartwig, 1995) and PKCα (Tigges et al., 2003) have also been shown to phosphorylate FLNa in vitro, although the phosphorylated residue has not been identified. Phosphorylation of FLNa affects its interaction with several proteins, and hence its actin binding and cross-linking activities (van der Flier and Sonnenberg, 2001), and prevents its cleavage by calpain (Chen and Stracher, 1989). In addition, FLNa phosphorylation regulates PAK1-mediated membrane ruffle formation (Vadlamudi et al., 2002) and EGF-induced cell migration (Woo et al., 2004).

Binding of Cav1 by FLNa has been detected (Stahlhut and van Deurs, 2000; Ravid et al., 2008; Sverdlov et al., 2009). Moreover, roles for FLNa in the trafficking of various cargoes have been identified. FLNa regulates albumin transcytosis across the endothelium (Sverdlov et al., 2009), opioid receptor trafficking (Onoprishvili et al., 2003), calcitonin receptor recycling (Seck et al., 2003), FcγRI subcellular distribution and signaling capacity (Beekman et al., 2008), and infection by SV40 and HIV (Jimenez-Baranda et al., 2007; Pelkmans et al., 2001). However, it remains unclear whether FLNa regulates caveolae trafficking and, if so, by what mechanism.

Here, we show that FLNa stabilizes Cav1 vesicles at the PM by linking them to the stress fibers, allowing them to be stably anchored to the cell surface. This FLNa-dependent linkage of Cav1 to actin fibers is required, but not sufficient, for proper inwards trafficking of caveolae triggered by loss of cell adhesion. Caveolae anchoring and inwards trafficking require FLNa–actin binding. Loss of cell adhesion induces a cycling phosphorylation of FLNa on Ser2152, which is also required for inwards trafficking of caveolae. This phosphorylation is regulated by at least one PKC isoform, PKCα, which is also required for cell-detachment-induced inwards trafficking of caveolae. Thus, PKCα-mediated FLNa phosphorylation regulates inwards trafficking of a pool of caveolae linked to actin filaments in an FLNa-dependent manner.

Results

Upon loss of cell adhesion, Cav1 internalizes and concentrates in a Rab11-positive perinuclear compartment

Cav1 is rapidly internalized upon cell detachment (del Pozo et al., 2004; del Pozo et al., 2005) and accumulates in an as yet uncharacterized perinuclear compartment. To confirm that Cav1 perinuclear distribution results from active internalization, rather than a blockade of exocytosis, we used time-lapse video microscopy to monitor the movement of GFP-labeled caveolae from the PM of suspended HeLa cells to the perinuclear compartment (Fig. 1A; supplementary material Movie 1). To identify the intracellular compartments, we stained cells with compartment markers: early endosome antigen 1 (EEA-1) (for early endosomes), GM130 (for the Golgi complex), pericentrin (for the microtubule organizer centre, MTOC) and Rab11 (for recycling endosomes, RE). The degree of colocalization between the internalized Cav1–GFP and each marker was calculated as the colocalization ratio (CR). In addition, GFP and marker intensity profiles were measured along a line drawn from the membrane across the cell through the Cav1–GFP distribution. Cav1–GFP and EEA-1 had very different intensity profiles and showed little overlap (CR=0.07±0.02). GM130 and pericentrin also gave low CRs (0.26±0.1 and 0.35±0.06), and had very different intensity profiles compared with Cav1–GFP. By contrast, Rab11 staining overlapped significantly with internalized Cav1–GFP (CR=0.7±0.08) and the two channels had very similar intensity profiles (Fig. 1B). The colocalization of these two markers was very low in adherent cells, whereas it increased with time in suspension (Fig. 1C).

FLNa regulates inwards trafficking of Cav1

To test whether FLNa plays a role in inwards trafficking of caveolae in response to cell detachment, we analyzed the behavior of Cav1 in FLNa-deficient (M2) and FLNa-reconstituted (A7) melanoma cells (Cunningham et al., 1992), which are widely used for the study of FLNa. M2 cells expressed no detectable endogenous Cav1 (Fig. 2A; supplementary material Fig. S1A,D); to enable us to study Cav1 trafficking we therefore expressed Cav1–Flag or Cav1–GFP in both cell lines. The levels of exogenously expressed Cav1–Flag or Cav1–GFP were similar in M2 and A7 cells (Fig. 2A; supplementary material Fig. S1A). Shortly after the detachment of A7 Cav1–Flag-expressing cells (A7-Cav1-Flag) (~0.25 minutes), most Cav1 remained at the cell periphery, close to or at the PM, consistent with studies in other cell types (del Pozo et al., 2005). Later (30 and 90 minutes), Cav1–Flag accumulated in the perinuclear compartment. By contrast, in M2 Cav1–Flag-expressing cells (M2-Cav1-Flag), most Cav1–Flag remained at the cell periphery, with a perinuclear distribution ~70% lower and ~50% lower than in A7-Cav1-Flag cells at 30 and 90 minutes of suspension, respectively (Fig. 2B,C). Similar results were obtained with A7 and M2 cells expressing Cav1–GFP (supplementary material Fig. S1B,C).

To confirm this result, we transiently knocked down FLNa in HeLa Cav1–GFP-expressing cells (HeLa-Cav1-GFP). Similar knockdown efficiencies were obtained after transfection with small interfering RNAs (siRNAs) for FLNa and for dynamin-2 (Dyn2), used as a positive control of internalization blockade (del Pozo et al., 2005) (Fig. 2D). After detachment of control cells, Cav1–GFP translocated from the PM to the perinuclear compartment. By contrast, FLNa knockdown inhibited caveolae translocation to the cell interior, similar to the effect of Dyn2 knockdown (Fig. 2E,F). Inhibition of inwards trafficking of Cav1–GFP was achieved with three additional FLNa siRNA oligonucleotides, thus excluding off-target effects (supplementary material Fig. S1F,G). To confirm these results for endogenous Cav1, we stably infected HeLa cells with short hairpin RNA (shRNA) against FLNa (HeLa-shFLNa cells) or against luciferase as a control (HeLa-shLuc cells) (Fig. 2H). Silencing of FLNa in this system blocked translocation of endogenous Cav1 to the perinuclear compartment and it was instead retained at the cell periphery (Fig. 2G,I). FLNa depletion had no significant effect on the distribution and amount of F-actin or on cell viability in suspension, whereas cell size was slightly increased (Fig. 2G; supplementary material Fig. S1H,I,J). The specificity of detachment-induced Cav1 internalization was confirmed by the lack of inwards trafficking of memb-cherry, a specific membrane marker (Megason and Fraser, 2003) (Fig. 2G). Although levels of filamin B (FLNb) and Cav2 were downregulated in M2 cells compared with their levels in A7 cells, FLNa-depletion in HeLa

cells did not affect expression of FLNb or caveolin-2 (Cav2) (supplementary material Fig. S2A,B,C). Transient FLNb knockdown with two independent siRNAs reduced inwards trafficking of Cav1 (supplementary material Fig. S2D,E; data not shown), suggesting that FLNb also modulates this process. The inability of both isoforms to compensate for each other suggests

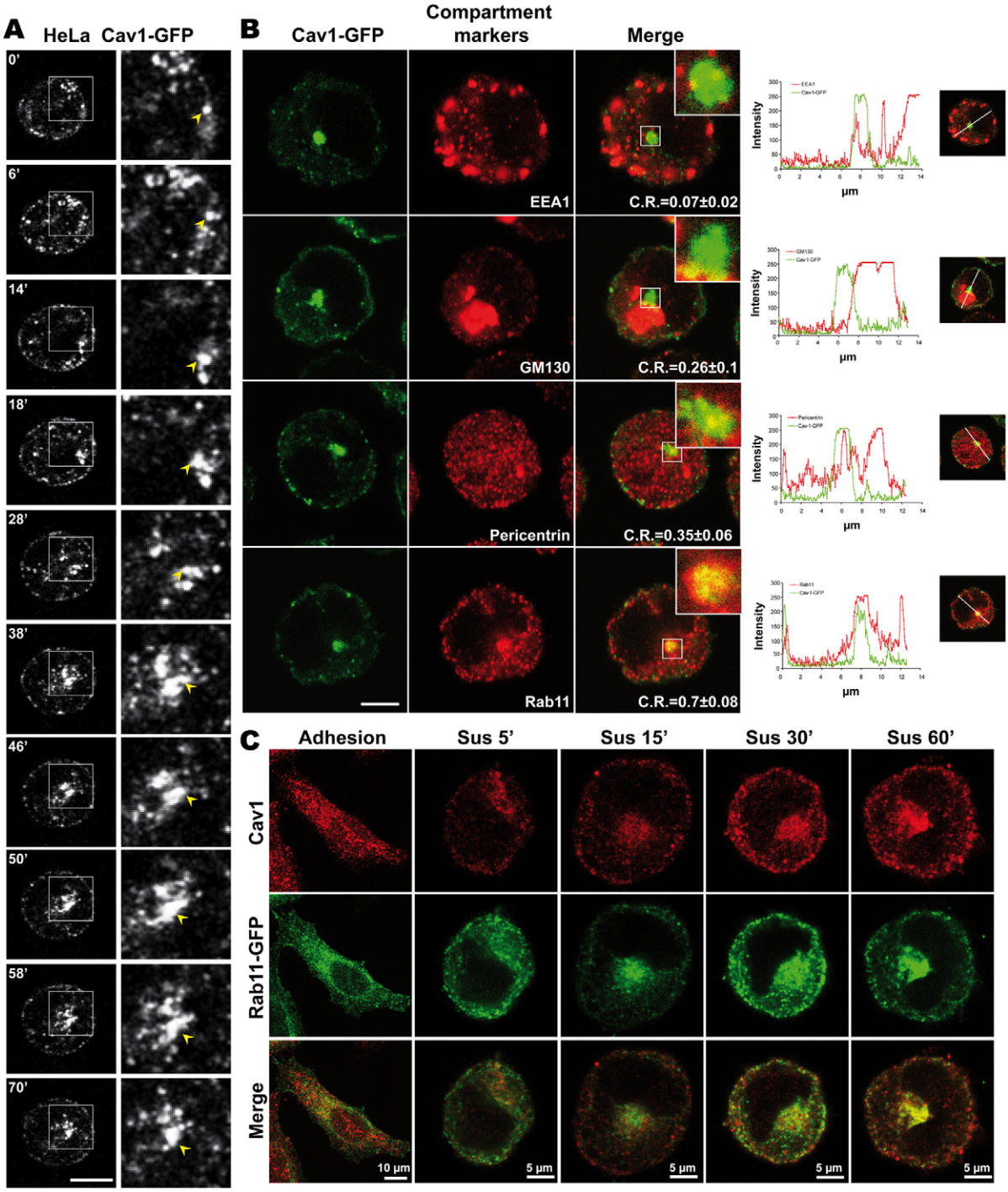

Fig. 1. Cav1–GFP is internalized to a recycling endosome after cell detachment. (**A**) Cav1–GFP traffics from the PM to the cell interior upon cell de-attachment. Panels show selected frames of a timelapse movie of HeLa-Cav1-GFP cells placed in suspension. Arrowheads mark a Cav1–GFP vesicle moving from the periphery to inside the cell. Scale bar: 10 µm. (**B**) Internalized Cav1–GFP colocalizes with a Rab11-positive RE compartment. HeLa-Cav1-GFP cells were placed in suspension for 60 minutes, fixed and stained with antibodies against cell compartment markers. The colocalization ratio (CR) between Cav1–GFP and the stained compartment was calculated using LAS AF software. Histograms show the fluorescence intensity profiles for compartment markers and Cav1–GFP across a cell diameter through the internalized Cav1–GFP intracellular focus, calculated with LAS AF software (see the Materials and Methods). Scale bar: 5 µm. (**C**) Colocalization of Cav1 and Rab11 occurs at longer suspension times. HeLa cells transiently transfected with Rab11–GFP were maintained adherent or in suspension for different times. Cells were then fixed and stained with anti-Cav1 antibody.

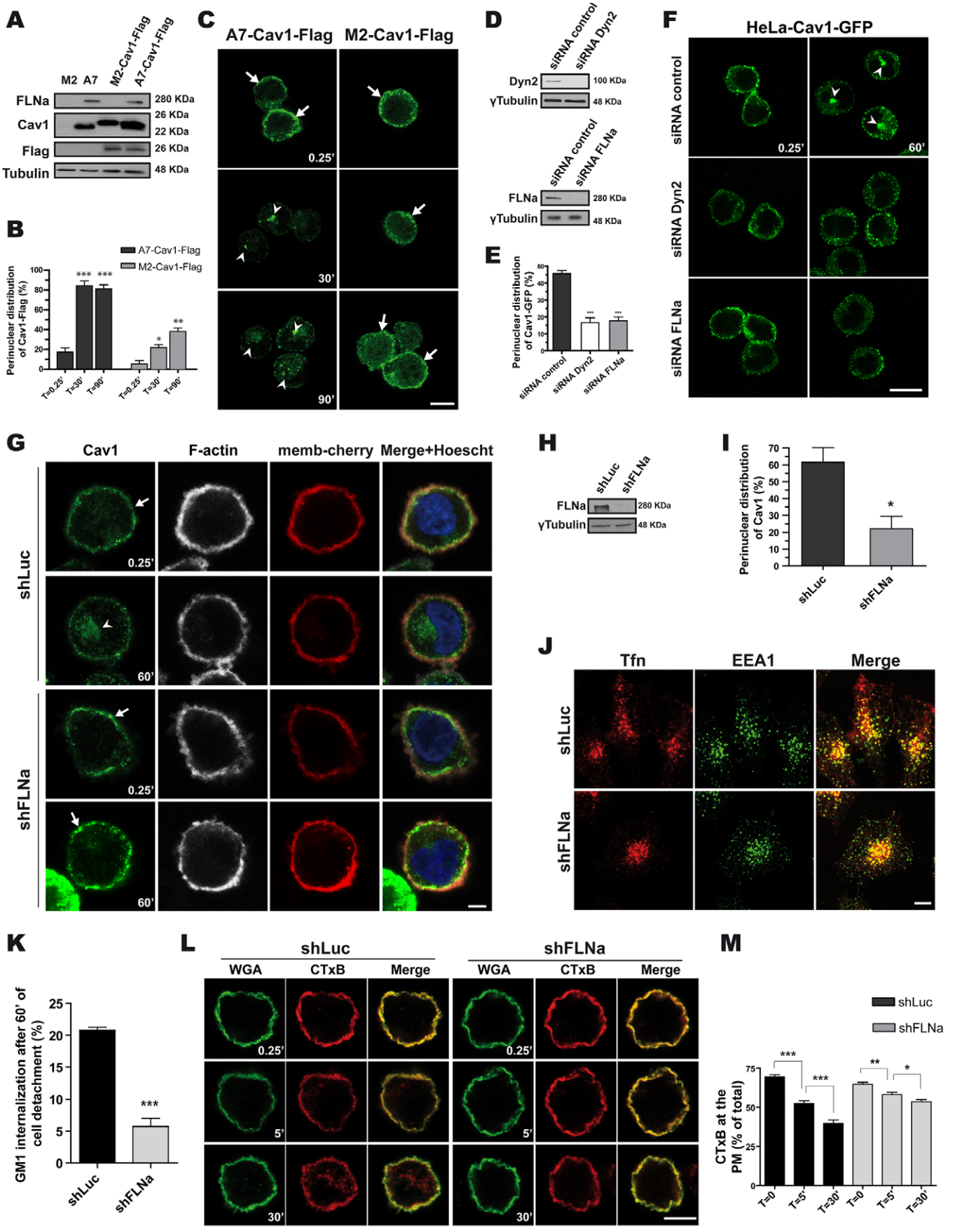

Fig. 2. See next page for legend.

that both are required for inwards trafficking of Cav1; in agreement, the FLNa and FLNb double-knockdown did not increase inwards trafficking of Cav1 compared with that of single knockdowns (supplementary material Fig. S2D,E). To investigate whether inwards trafficking of Cav1 was also regulated by other actin crosslinking proteins, we analyzed the localization of Cav1–GFP in suspended HeLa cells transiently depleted of the non-muscle α-actinin isoforms 1 and 4 (supplementary material Fig. S2F). The perinuclear distribution of Cav1–GFP after α-actinin-1 and 4 depletion with three different siRNAs was similar to that observed in control cells (supplementary material Fig. S2G,H), supporting the specific function of filamins in the regulation of this process.

To confirm the defect on inwards trafficking of Cav1 in FLNa-depleted HeLa cells, we exposed detached cells to cholera toxin subunit B (CTxB) in order to detect the amount of GM1 remaining at the PM. CTxB is one of the few cargos identified to enter through caveolae (Parton, 1994) and, although it also internalizes through other pathways (Howes et al., 2010), its entry is preferentially Cav1-dependent upon cell detachment (del Pozo et al., 2005) (Balasubramanian et al., 2007). GM1 internalization, measured by FACS after 60 minutes in suspension, was significantly decreased in the absence of FLNa (Fig. 2K). This result is supported by immunofluorescence experiments in cells treated with CTxB before detachment; in control cells, PM CTxB decreased progressively after detachment. However, in HeLa-shFLNa cells CTxB internalization was delayed (Fig. 2L,M), suggesting that FLNa regulates the first step of CTxB entry. Defects in CTxB uptake were also observed in M2 cells (supplementary material Fig. S1E). FLNa knockdown had no effect on transferrin (Tfn) uptake, indicating that the effects on CTxB uptake are unrelated to Cav1-independent entry through clathrin-mediated endocytosis (Fig. 2J). FLNa thus appears to play a crucial and specific role in the first steps of inwards trafficking of Cav1.

Fig. 2. FLNa regulates inwards trafficking of Cav1 and CTxB in a clathrin-independent manner. (**A**) Western blots of extracts from M2, A7, M2-Cav1-Flag and A7-Cav1-Flag cells were probed with anti-FLNa, anti-Cav1 and anti-Flag antibodies. γ-tubulin was used as a loading control. (**B**) Inwards trafficking of Cav1 was quantified as the percentage of cells containing perinuclear Cav1–Flag. Data are means ± s.e.m. (n=3). (**C**) M2-Cav1-Flag and A7-Cav1-Flag cells were placed in suspension and stained for Cav1 after 0.25, 30 and 90 minutes. Confocal images show that Cav1–Flag is internalized in A7-Cav1-Flag cells but remains at the cell periphery in M2-Cav1-Flag cells. Arrows mark peripheral Cav1–Flag distribution. Arrowheads mark perinuclear Cav1–Flag distribution. (**D**) Western blots showing the effect of Dyn2 and FLNa siRNAs on target protein expression in Cav1–GFP-expressing HeLa cells 48 hours post transfection. γ-tubulin was used as a loading control. (**E**) Inwards trafficking of Cav1 after 60 minutes suspension was quantified as the percentage of cells containing perinuclear Cav1–GFP. Data are means ± s.e.m. (n=4). (**F**) HeLa-Cav1-GFP cells transfected with control, Dyn2 or FLNa siRNAs were detached (48 hours post transfection) and placed in suspension, and the localization of Cav1–GFP was monitored at 0.25 and 60 minutes. Arrowheads mark Cav1–GFP perinuclear distribution. (**G**) HeLa-shFLNa and HeLa-shLuc cells expressing memb-cherry, were detached, fixed after 0.25 or 60 minutes, permeabilized and stained for endogenous Cav1 and F-actin. Arrows mark peripheral distribution of endogenous Cav1. Arrowheads mark endogenous Cav1 perinuclear distribution. (**H**) The western blot shows the effect of FLNa shRNA on target protein expression. γ-tubulin was used as a loading control. (**I**) Inwards trafficking of Cav1 after 60 minutes of suspension was quantified as the percentage of cells with perinuclear Cav1 staining. Data are means ± s.e.m. (n=3). (**J**) FLNa is not required for Tfn uptake. HeLa-shFLNa and HeLa-shLuc cells were incubated with Tfn for 15 minutes, and fixed and stained with an anti-EEA1 antibody. Tfn concentrated inside the cell in both cases. (**K**) FLNa is required for GM1 internalization in suspension. HeLa-shLuc and HeLa-shFLNa cells were placed in suspension for 0.25 and 60 minutes, incubated with 8 ng/μl of CTxB conjugated to Alexa Fluor 647 and fixed with 2% PFA. The non-internalized GM1 was measured by FACS and the percentage of GM1 internalization is shown. Data are means ± s.e.m. (n=3). (**L**) FLNa is required for CTxB uptake in HeLa cells. HeLa-shFLNa and HeLa-shLuc cells were incubated with CTxB at 4°C and maintained in suspension as indicated. Wheat germ agglutinin (WGA) was used as a PM marker. (**M**) Quantification of CTxB at the PM (see the Materials and Methods). Data are means ± s.d. *P≤0.05; **P≤0.01; ***P≤0.005. Scale bars: 10 μm (C,F,L); 5 μm (G); 7.5 μm (J).

FLNa regulates the distribution and anchorage of Cav1 along actin stress fibers

Upon RhoA activation, Cav1 adopts a linear distribution, co-aligning with actin fibers in FLNa-positive patches (Stahlhut and van Deurs, 2000). To investigate whether FLNa is necessary to maintain this distribution, we analyzed these linear Cav1 structures in attached HeLa-shFLNa cells. Linear Cav1 distribution was identified in HeLa-shLuc control cells (Fig. 3A), but was less evident in shFLNa cells (Fig. 3A; supplementary material Fig. S3I). FLNa depletion has been reported not to affect dramatically the actin cytoskeleton structure and stress fiber disposition (Baldassarre et al., 2009; Feng et al., 2006; Sverdlov et al., 2009). Nonetheless, under adherent conditions the stress fibers appear to be different between HeLa-shLuc and HeLa-shFLNa cells (Fig. 3A). We therefore transfected these cell lines with a constitutively active RhoA mutant (RhoAG14V) in order to rule out a possible effect of FLNa knockdown on RhoA-dependent actin dynamics (supplementary material Fig. S3A). RhoAG14V expression increased the alignment of Cav1 on stress fibers in both cell lines (data not shown); however, the linear pool remained lower in cells lacking FLNa (Fig. 3B; supplementary material Fig. S3B), indicating that the alterations in stress fibers cannot account for the effect of FLNa knockdown on Cav1 distribution. To verify that the linear Cav1 distribution requires actin, we analyzed endogenous Cav1 distribution in RhoA-silenced HeLa cells. RhoA depletion caused a marked alteration of the actin cytoskeleton, with a reduction in the number of stress fibers and in linear Cav1. Two additional RhoA siRNA oligonucleotides gave similar results (supplementary material Fig. S3C,D,E). The specific requirement of FLNa over the RhoA effect was validated by the absence of rescue of inwards trafficking of Cav1 in HeLa-shFLNa cells after RhoAG14V expression (supplementary material Fig. S3F,G).

To understand how FLNa regulates linear Cav1 distribution, we studied the effect of FLNa depletion on caveolae at the PM. The penetration depth of total internal reflection fluorescence (TIRF) microscopy (TIRFm) allowed us to specifically monitor those Cav1–GFP vesicles close to the PM. We set the TIRFm depth to 90 nm, which compares with a vesicle diameter of about 100 nm, suggesting that the identified Cav1–GFP puncta could be vesicles. In sequences of 1000 images of attached shLuc cells, the observed Cav1–GFP vesicles remained in this thin layer for almost the entire duration of the movie (~2 minutes). The Cav1–GFP vesicles appear as well-separated spots (supplementary material Movies 2, 3); moreover, their size distribution, analyzed in a similar way to that described previously (Pelkmans and Zerial, 2005) (supplementary material Fig. S4A,B), is characteristic of non-aggregated vesicles. Knockdown of FLNa did not alter Cav1–GFP vesicle size or population distribution (supplementary material Fig. S4A,B). Subtraction of subsequent frames of the TIRFm movies suggested

that Cav1–GFP vesicle movement over periods of 30 seconds and above was similar in the presence or absence of FLNa (supplementary material Fig. S4C,D).

To study lateral Cav1–GFP vesicle mobility more precisely, we used a single-particle tracking approach to monitor individual Cav1–GFP vesicle trajectories in shFLNa and shLuc cells. This

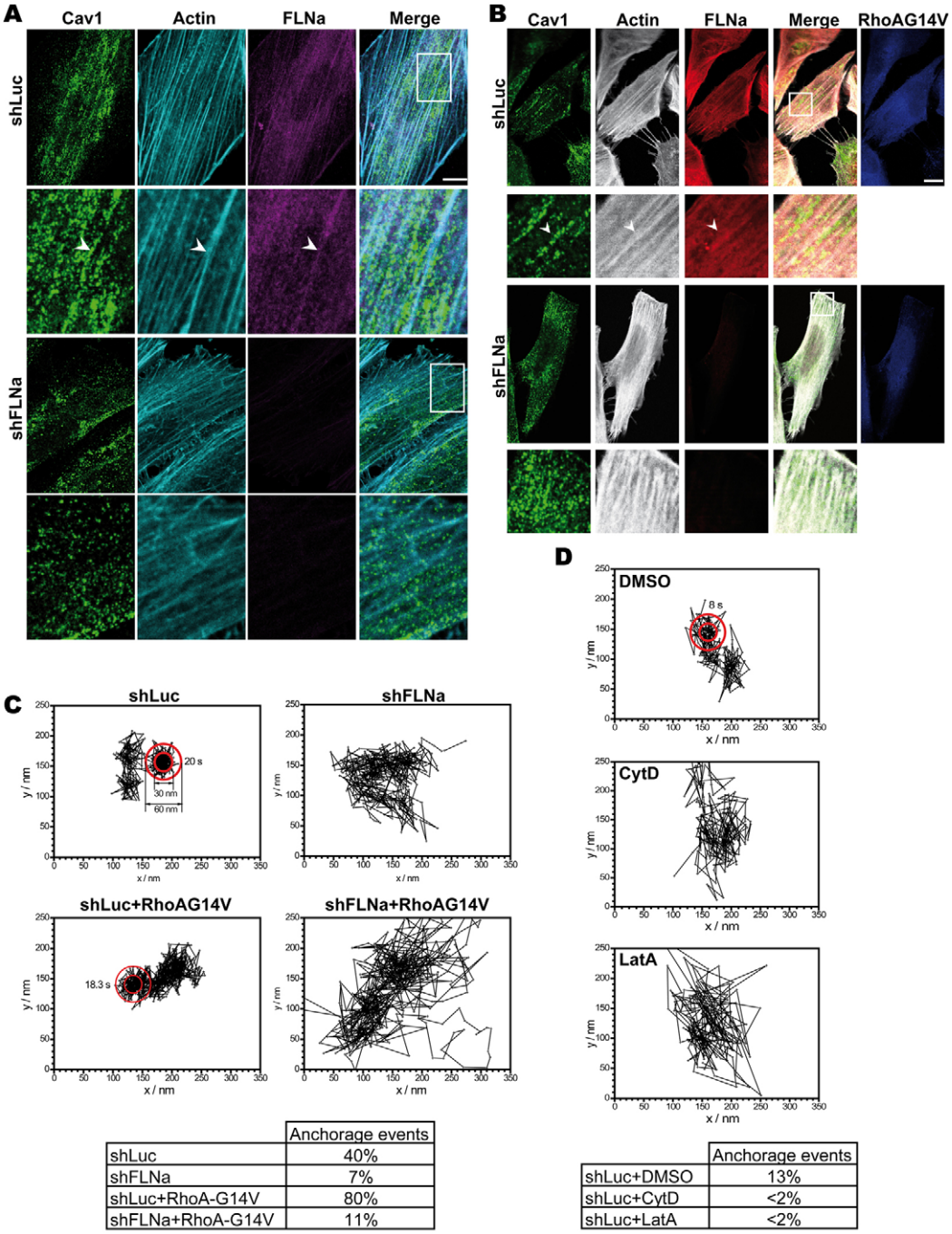

	Anchorage events
shLuc	40%
shFLNa	7%
shLuc+RhoA-G14V	80%
shFLNa+RhoA-G14V	11%

	Anchorage events
shLuc+DMSO	13%
shLuc+CytD	<2%
shLuc+LatA	<2%

Fig. 3. FLNa regulates a Cav1 pool that is linked and anchored to actin fibers. (**A**) FLNa depletion reduces the linear distribution of endogenous Cav1 co-aligned with actin fibers. Cells were stained for Cav1, FLNa and F-actin. Arrowheads mark the aligned Cav1 pool overlapping with an actin filament and with FLNa staining in shLuc control cells. (**B**) FLNa depletion reduces RhoAG14V-induced co-alignment of endogenous Cav1 with actin fibers. Constitutively active GFP-tagged RhoAG14V was transiently expressed in HeLa-shFLNa and HeLa-shLuc cells to stimulate alignment of Cav1 vesicles with actin fibers. Arrowheads mark aligned Cav1 overlapping with an actin filament and FLNa staining. Image colors were selected to facilitate visualization. (**C**) Typical trajectories of Cav1–GFP vesicles in HeLa-shFLNa and HeLa-shLuc cells and the same cells expressing RhoAG14V–cherry. Sequential vesicle positions were recorded at 85 ms intervals and connected by straight lines. Outer circles show the threshold for an anchoring event (60-nm diameter); inner circles show the positioning accuracy (30-nm diameter). Duration of anchoring events is indicated on the figure. The table gives the percentage of tracks showing anchoring events for all conditions (30 trajectories per cell, five cells per condition, n=3 or 4). (**D**) Typical trajectories of Cav1–GFP vesicles in HeLa cells treated with CytD (1 μM) and LatA (1 μM). The same volume of DMSO was used as a control. The table gives the percentage of tracks showing anchoring events for all conditions (30 trajectories per cell, five cells per condition, n=3). Scale bars: 10 μm.

approach gives a spatiotemporal resolution of 30 nm and 85 ms. Approximately 97% of Cav1–GFP vesicles were stable, showing slow movement over short distances, with the remaining 3% showing pronounced long-range directional active-transport sprints (supplementary material Movies 2, 3). This agrees with previous observations using fluorescence recovery after photobleaching (FRAP) (Thomsen et al., 2002), TIRFm (Pelkmans and Zerial, 2005; Sverdlov et al., 2009; Tagawa et al., 2005) and spinning disc confocal microscopy (McMahon et al., 2009). The main difference between shFLNa and shLuc cells was in the motion of the slow-moving more-localized vesicles over short timescales (~10 seconds or less). Cav1–GFP vesicle movements in shLuc control cells were more confined, with many remaining immobile to within the positioning accuracy (on average 30 nm) for periods of 5–10 seconds. To quantify this observation, we defined an anchoring event as mobility limited within a radius of 30 nm for at least 4.7 seconds (see Materials and Methods), and found that 40% of Cav1–GFP vesicles in shLuc control cells showed at least one anchoring event (Fig. 3C; supplementary material Fig. S5). Only 7% of Cav1 vesicles in shFLNa cells showed anchoring, with almost all showing jittery movement within a confined area (Fig. 3C; supplementary material Fig. S5). Thus, Cav1–GFP vesicle movement in the absence of FLNa was essentially chaotic, whereas in control cells these vesicles moved between anchoring points in a 'stop-and-go'-like manner.

Because linear caveolae distribution positively correlated with RhoA activity, we tested the effect of constitutively active RhoA on the anchoring of Cav1 vesicles. Expression of the active RhoAG14V mutant doubled the incidence of Cav1 anchorage in shLuc control cells (to 80%), but had little effect on the number of anchoring events in shFLNa cells (11%) (Fig. 3C; supplementary material Fig. S5). Thus RhoA facilitates FLNa-dependent perimembranous anchorage of Cav1 vesicles, probably by regulating the function and stability of actin stress fibers. To validate the involvement of the actin cytoskeleton in Cav1 anchoring, already suggested by the effect of RhoAG14V, we analyzed Cav1 anchoring after treatment with cytochalasin D (CytD) or latrunculin A (LatA). Both drugs decreased the number of the anchoring events ~sixfold (Fig. 3D). To discount a general effect of FLNa on membrane proteins, we studied the effect of FLNa depletion on the PM marker (memb-cherry). The anchoring dynamics of this PM marker differed from Cav1 and was not affected by the absence of FLNa, indicating that actin-dependent Cav1 membrane anchoring is specifically mediated by FLNa (supplementary material Fig. S4E). Moreover, knockdown of both α-actinin-1 and α-actinin-4 together did not affect Cav1 anchoring, suggesting the specificity of FLNa in the regulation of these dynamics (supplementary material Fig. S4F).

Binding of FLNa to actin and its phosphorylation at Ser2152 are required for Cav1 distribution in adherent cells

Because the actin cytoskeleton regulates Cav1 dynamics, we wondered whether FLNa regulation of Cav1 was mediated by its ability to bind actin. Given that phosphorylation at Ser2152 is involved in many FLNa-regulated processes (Stossel et al., 2001), we analyzed the effect of this phosphorylation on Cav1 dynamics. We constructed three mutants from a dsRED-tagged shRNA-resistant FLNa wild-type (WT) construct (FLNa-shRNA^{R}WT): an actin-binding domain deletion (FLNa-shRNA^{R}ABD), a non-phosphorylatable mutant (FLNa-shRNA^{R}S2152A), and a phosphomimetic mutant (FLNa-shRNA^{R}S2152E) (Fig. 4A). Western blot confirmed that all three mutants were expressed at similar levels to FLNa-shRNA^{R}WT, but only FLNa-shRNA^{R}ABD was phosphorylated (Fig. 4B).

The suppressed anchoring in FLNa-depleted cells was rescued by expression of FLNa-shRNA^{R}WT (41.6%). Expression of FLNa-shRNA^{R}S2152A increased anchoring above the level in control

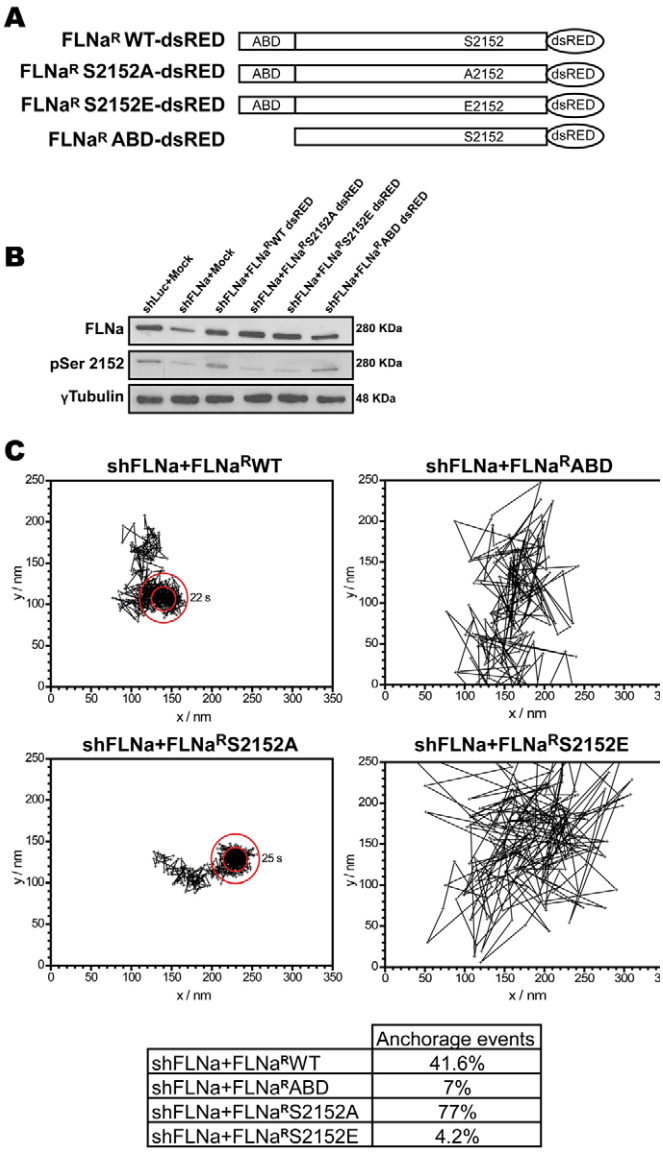

	Anchorage events
shFLNa+FLNa^{R}WT	41.6%
shFLNa+FLNa^{R}ABD	7%
shFLNa+FLNa^{R}S2152A	77%
shFLNa+FLNa^{R}S2152E	4.2%

Fig. 4. FLNa binding to actin and FLNa (Ser2152) phosphorylation dynamics regulate Cav1 anchoring. (**A**) Schematic drawing showing FLNa WT and three different mutants. ABD, actin-binding domain. (**B**) Western blot of extracts of shFLNa and shLuc cells transfected with mock plasmid (mRFP), FLNa-shRNA^{R}WT, FLNa-shRNA^{R}S2152A, FLNa-shRNA^{R}S2152E or FLNa-shRNA^{R}ABD. Blots were probed with anti-FLNa and anti-phosphoFLNa (Ser2152) antibodies. γ-tubulin was used as a loading control. (**C**) Typical trajectories of Cav1–GFP vesicles in HeLa-shFLNa cells expressing FLNa-shRNA^{R}WT, FLNa-shRNA^{R}ABD, FLNa-shRNA^{R}S2152A and FLNa-shRNA^{R}S2152E. The table gives the percentage of tracks showing anchoring events for all conditions (30 trajectories per cell, five cells per condition, n=3 or 4).

cells (77%), whereas expression of FLNa-shRNA^{R}S2152E or FLNa-shRNA^{R}ABD had no effect (Fig. 4C; supplementary material Fig. S5). Moreover, FLNa-shRNA^{R}-S2152A, but not FLNa-shRNA^{R}-S2152E or FLNa-shRNA^{R}-ABD, was just as effective at restoring the linear Cav1 distribution as the WT form (supplementary material Fig. S3H,I), correlating with the anchoring results. This suggests that FLNa links Cav1 and actin in a manner regulated by phosphorylated Ser2152.

Binding of FLNa to actin and its phosphorylation at Ser2152 regulate inwards trafficking of Cav1 in suspended cells

The results presented so far indicate that FLNa-dependent Cav1 anchorage and linear distribution require actin binding by FLNa and its phosphorylation on Ser2152. To study the role of this phosphorylation in inwards trafficking of Cav1 during cell detachment, we analyzed adhered and detached cells. Attached cells showed a basal level of phosphorylated FLNa (Ser2152), which increased after 5 minutes in suspension (increment of 1.629±0.097) but returned to basal levels after prolonged suspension (60 minutes) (Fig. 5A). This suggests that increased Ser2152 phosphorylation plays a role in the first steps of inwards trafficking of Cav1. To explore this further, we monitored FLNa localization. Shortly after cell detachment (~0.25 minutes), Cav1 and FLNa were at the cell periphery, close to the PM. After a longer suspension, most Cav1 translocated towards the perinuclear compartment, whereas FLNa remained at the cell periphery (Fig. 5B). To test the potential role of Ser2152 phosphorylation in inwards trafficking of Cav1, we expressed non-phosphorylatable and phosphomimetic shRNA-resistant FLNa in shFLNa cells. Perinuclear distribution of Cav1–GFP was 40% lower in shFLNa cells than in shLuc control cells (Fig. 5C,D). Perinuclear Cav1 distribution was restored by the introduction of FLNa-shRNA^{R}WT but not by any of the Ser2152 or ABD deletion mutants (Fig. 5C,D).

Inwards trafficking of Cav1–GFP requires PKCα-mediated phosphorylation of FLNa

Among the several kinases that phosphorylate FLNa (Stossel et al., 2001), PKCα localizes to caveolae (Smart et al., 1995; Tigges et al., 2003) and PKA is activated by cell detachment (Howe and Juliano, 2000; Jay et al., 2004). The PKA inhibitor H-89 did not

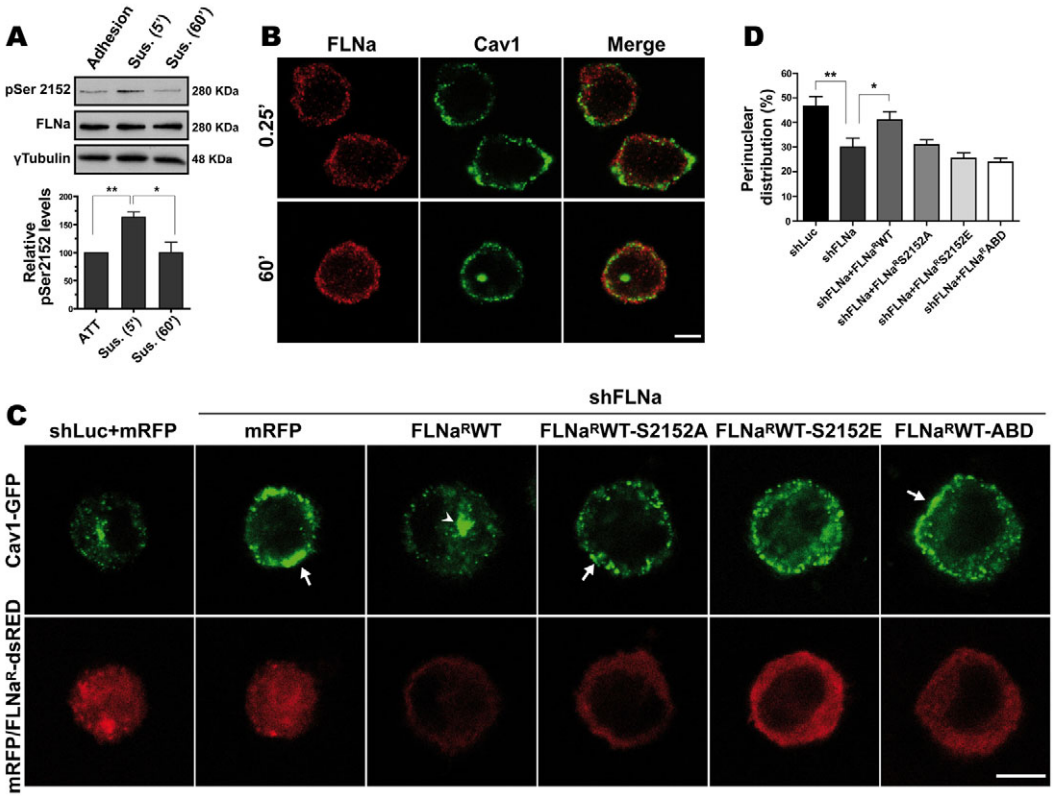

Fig. 5. FLNa binding to actin and cycling of FLNa (Ser2152) phosphorylation are required for inwards trafficking of Cav1–GFP. (**A**) Loss of cell adhesion induces FLNa Ser2152 phosphorylation. Cav1–GFP-expressing HeLa cells were kept adherent (Adhesion) or suspended (Sus.) for 5 or 60 minutes. Western blots show levels of phosphorylated FLNa Ser 2152 (pSer 2152) and total FLNa. γ-tubulin was used as a loading control. The bar chart shows densitometric quantification of Ser2152 phosphorylation (Quantity one software; n=3). (**B**) FLNa does not colocalize with perinuclear Cav1–GFP. HeLa-Cav1-Flag cells were placed in suspension for 0.25 or 60 minutes, and then stained for FLNa. Confocal images show localization of Cav1–GFP and FLNa close to the PM at 0.25 minutes and perinuclear distribution of Cav1–GFP but retention of FLNa at the cell periphery after 60 minutes. (**C**) FLNa Ser2152 phosphorylation and FLNa–actin binding regulates inwards trafficking of Cav1. Confocal images after 60 minutes of suspension show perinuclear distribution of Cav1–GFP in HeLa-shLuc cells but not in HeLa-shFLNa cells expressing a mock (mRFP). Expression of FLNa-shRNA^{R}WT, but not FLNa-shRNA^{R}ABD, FLNa-shRNA^{R}S2152A or FLNa-shRNA^{R}S2152E, restored inwards trafficking of Cav1–GFP in shRNA-FLNa cells. Arrows mark peripheral distribution of Cav1–GFP. Arrowheads mark perinuclear distribution of Cav1–GFP. (**D**) Inwards trafficking of Cav1–GFP was quantified as the percentage of cells containing perinuclear Cav1–GFP under different conditions. Data are means ± s.e.m. (n=8). Scale bars: 5 μm (B); 7.5 μm (C). *P≤0.05; **P≤0.01.

significantly affect the increase in Ser2152 phosphorylation detected after 5 minutes of suspension (Fig. 6A). By contrast, the increase was completely inhibited by treatment with Ro-31-8229, a non-isoform specific PKC inhibitor (Fig. 6B), and with Gö6976, which inhibits conventional PKC isoforms (Fig. 6C). Treatment of HeLa-Cav1-GFP cells with either of these inhibitors prevented detachment-induced inwards trafficking of Cav1–GFP (Fig. 6D). Detachment-induced Ser2152 phosphorylation and inwards trafficking of Cav1–GFP were also inhibited by expression of two PKCα-specific siRNAs (Fig. 6E,F; supplementary material Fig. S6). Examination of PKC expression confirmed reduced levels of PKCα but not of PKCδ or PKCε (supplementary material Fig. S6C).

FLNa-mediated Cav1 retention at the PM regulates Rac1 targeting and cell proliferation

To determine whether the defective inwards trafficking of Cav1 in FLNa-depleted cells correlated with alterations in Cav1-regulated signaling, we measured the localization of Rac1, because Cav1 internalization causes entry of Rac1-binding sites via caveolae (del Pozo et al., 2005). Whereas Rac1 expression levels were unaffected by FLNa knockdown (Fig. 7A), after 1 hour of suspension FLNa-silenced cells retained Rac1 at the cell periphery, contrasting with the homogenous cytosolic distribution in control cells (Fig. 7B,C). Rac1 PM targeting was also prominent in shFLNa cells during spreading (Fig. 7D). Localization of Rac1 at the PM was accompanied by activation of its downstream effector PAK,

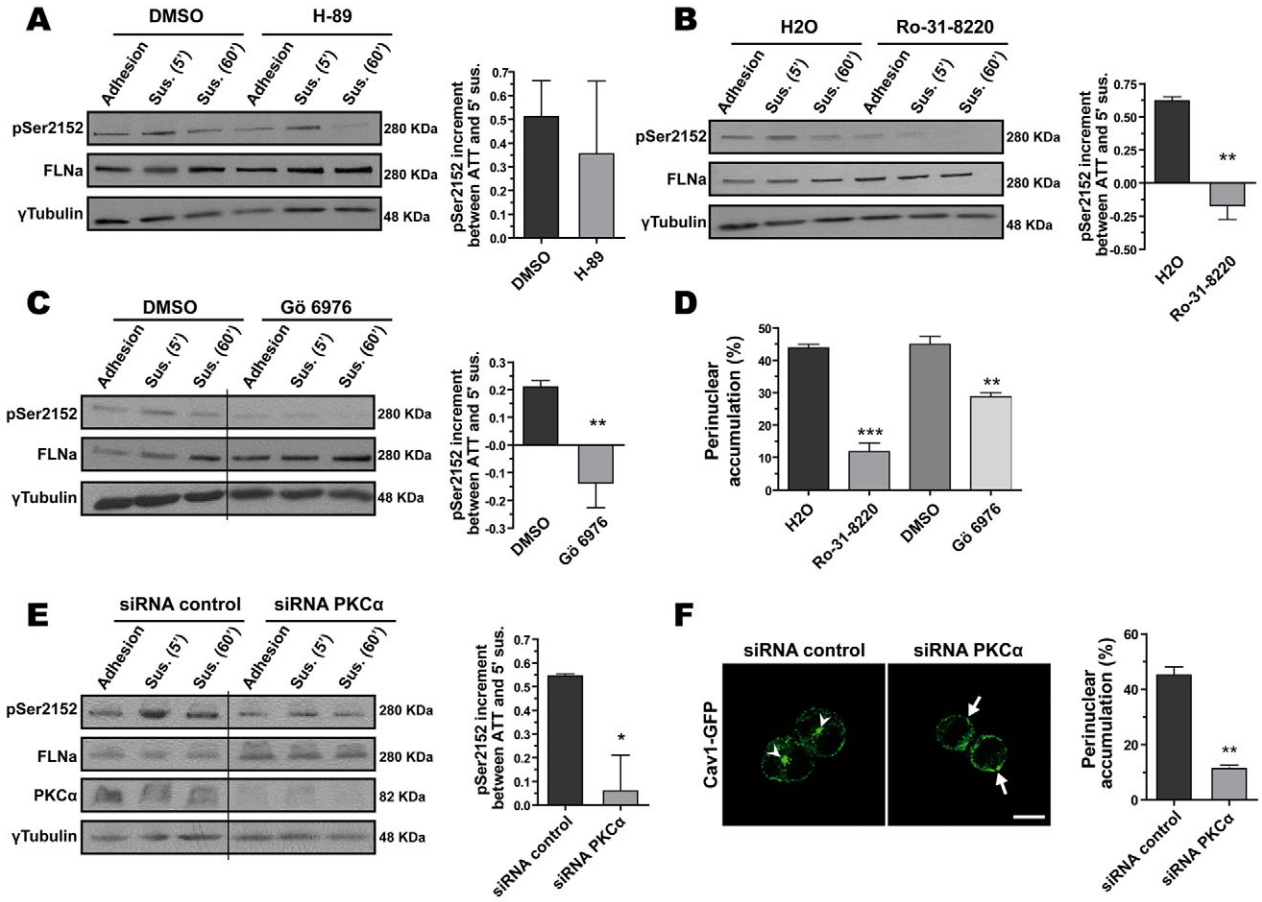

Fig. 6. PKCα is required for FLNa phosphorylation and inwards trafficking of Cav1–GFP. (**A**) PKA inhibition does not alter FLNa Ser2152 phosphorylation. The increase in FLNa phosphorylation on Ser2152 after 5 minutes of suspension was not affected by treatment with the PKA inhibitor H-89. Adhered HeLa-Cav1-GFP cells were treated with 10 μM H-89 or DMSO for 30 minutes and either kept adherent (Adhesion) or suspended (Sus.) for 5 or 60 minutes, in the continued presence of H-89 or DMSO. Cell lysates were blotted for phosphorylated FLNa (Ser2152) (pSer2152) and FLNa. γ-tubulin was used as a loading control. FLNa phosphorylation levels at Ser2152 were quantified by densitometry (Quantity one software). The bar chart shows the change in Ser2152 phosphorylation, calculated as the ratio between the adhesion and 5-minute suspension band intensities (n=3). (**B**) PKC regulates FLNa Ser2152 phosphorylation. The procedure described in A was repeated with the general PKC inhibitor Ro-31-8220 (10 μM). (**C**) Conventional PKC isoforms regulate FLNa Ser2152 phosphorylation. The procedure described in A and B was repeated with the conventional-subtype-specific PKC inhibitor Gö 6976 (5 μM). The dividing line reflects two areas of the same gel. (**D**) PKC regulates de-adhesion induced inwards trafficking of Cav1–GFP. HeLa-Cav1-GFP cells were treated with Ro-31-8220, Gö 6976 or DMSO as indicated and placed in suspension for 60 minutes. Inwards trafficking of Cav1–GFP was quantified as the percentage of cells containing perinuclear Cav1–GFP (n=3). (**E**) PKCα regulates FLNa Ser2152 phosphorylation. HeLa-Cav1-GFP cells expressing control or PKCα siRNA were maintained in adhesion or placed in suspension and processed as in A–C. The dividing line reflects two areas of the same gel (n=3). (**F**) PKCα regulates de-adhesion induced Cav1-GFP inward trafficking. HeLa Cav1-GFP cells expressing control or PKCα siRNA were placed in suspension for 60 minutes and the localization of Cav1–GFP was monitored. Arrows mark peripheral Cav1–GFP distribution; arrowheads mark perinuclear Cav1–GFP distribution. Inwards trafficking of Cav1–GFP was quantified as the percentage of cells containing perinuclear Cav1–GFP. Data are means ± s.e.m. *P≤0.05; **P≤0.01; ***P≤0.005. Scale bar: 10 μm.

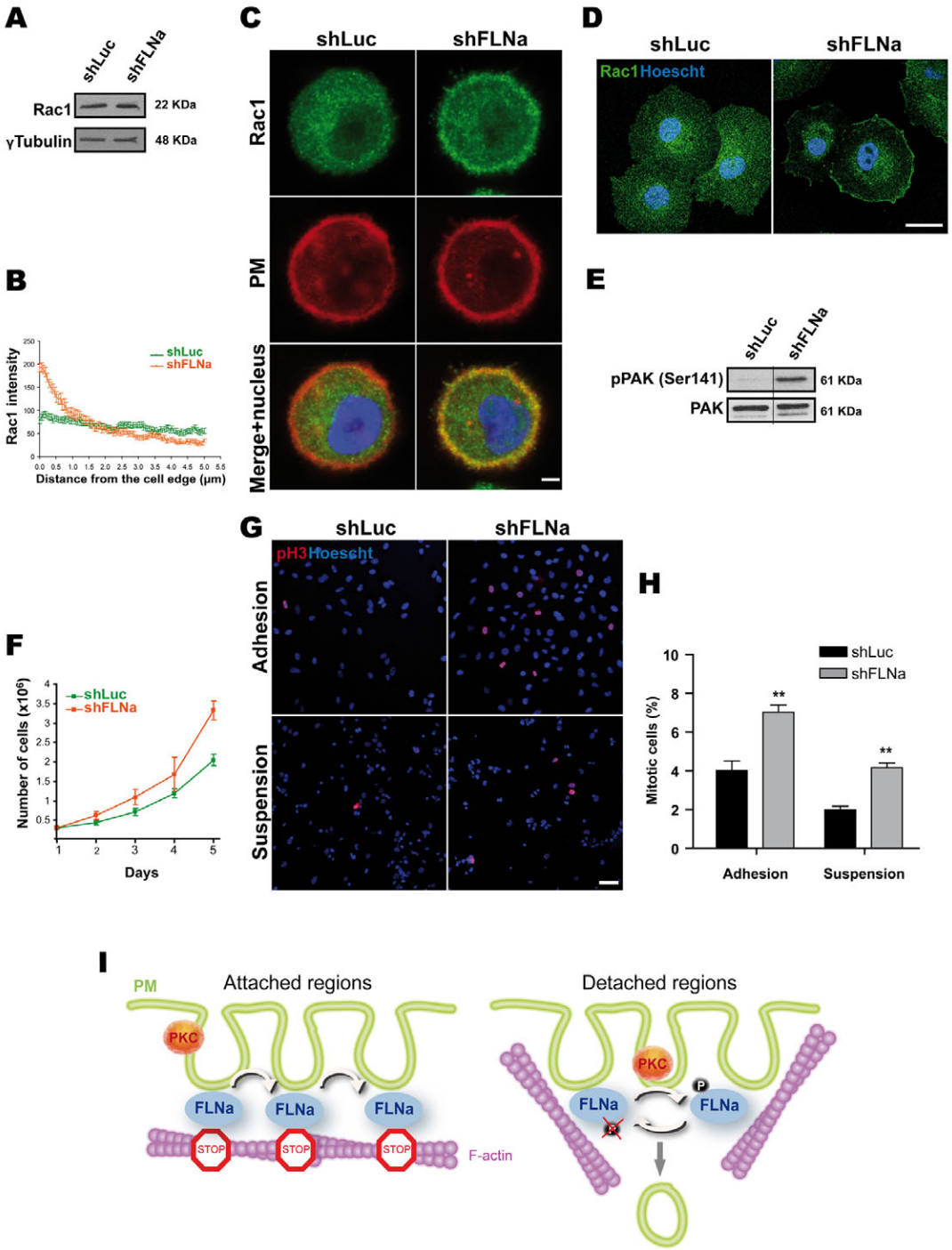

Fig. 7. FLNa depletion regulates Rac1 signaling and proliferation. (**A**) The western blot confirms similar expression levels of Rac1 in HeLa-shLuc and HeLa-shFLNa cells. γ-tubulin was used as a loading control. (**B**) The chart shows Rac1 staining intensity measured at 5-μm intervals from the cell edge to the interior. (**C**) FLNa is required for release of endogenous Rac1 from the PM. HeLa-shFLNa and HeLa-shLuc cells expressing a membrane marker were placed in suspension, fixed after 60 minutes, permeabilized and stained for Rac1. (**D**) Rac1 PM targeting is more prominent in shFLNa cells during spreading. HeLa-shFLNa and HeLa-shLuc cells were placed in suspension for 60 minutes, re-plated on fibronectin for 20 minutes, to allow spreading, and then fixed and stained for Rac1. (**E**) PAK remains phosphorylated on Ser141 in HeLa-shFLNa cells after 60 minutes of suspension. Cell lysates were blotted for phosphorylated PAK (Ser141) (pPAK) and PAK1. The dividing line reflects two areas of the same gel. (**F**) Cells cultured in medium containing 2% serum were trypsinized and counted in a counter (CASY Model TT; Roche Applied Science). The results are given as mean values at 2–5 days in triplicates at each observation time. (**G**) HeLa-shLuc and HeLa-shFLNa cells were kept adherent or suspended for 20 hours. Cells were then fixed and stained for phosphorylated histone 3 (pH3) and nucleus. (**H**) The percentage of cells with phosphorylated histone 3 staining is represented. Data are means ± s.d. (n=3). (**I**) Model of FLNa-mediated inwards trafficking of actin-linked caveolae downstream of PKC. FLNa anchors caveolae at the PM by linking them to actin fibers. Shortly after cell detachment, PKC phosphorylates FLNa and then FLNa phosphorylation returns to the basal levels. These the FLNa phosphorylation and dephosphorylation cycle enables inwards trafficking of Cav1 towards a RE. **P≤0.01. Scale bars: 5 μm (C); 25 μm (D); 50 μm (G).

observed in suspended shFLNa cells (Fig. 7E). Levels of PAK phosphorylation at Ser141 were used to measure PAK activity (Parrini et al., 2009). Rac1 signaling is responsible for increased cell proliferation and anchorage-independent growth in the absence of caveolae internalization (Cerezo et al., 2009). The rate of cell proliferation was increased in adherent FLNa-silenced cells (Fig. 7F), an effect which appears to be secondary to an increase in the number of mitotic cells, measured by staining for phosphorylated histone 3 (Fig. 7G,H). The mitosis rate was also increased in suspended cells upon FLNa knockdown (Fig. 7G,H). Therefore, the effect of FLNa on caveolae internalization has subsequent effects on the targeting of signaling molecules, such as Rac1, which in turn regulate anchorage-dependent and -independent cell proliferation.

Discussion

Here, we show that FLNa is involved in Cav1 dynamics at three levels. First, FLNa regulates the linear distribution of Cav1 along actin stress fibers. Second, it regulates the anchoring of Cav1 vesicles at the PM. Third, it is required for Cav1 translocation from the PM to colocalize with perinuclear Rab11. All these functions are regulated by the phosphorylation state of FLNa on Ser2152 and its ability to bind F-actin. Previous studies have shown co-alignment of Cav1 with the actin cytoskeleton, but how this association is mediated was not reported (Stahlhut and van Deurs, 2000). Our results indicate that FLNa-mediated association of Cav1 with actin is necessary for inwards trafficking of Cav1.

Despite the fact that M2 and A7 cells differ radically in morphology and actin distribution, single FLNa knockout (Feng et al., 2006) and knockdown cells – either endothelial (Sverdlov et al., 2009) or HT1080 (Baldassarre et al., 2009) – do not differ greatly from WT cells or cells with no interference in their general actin cytoskeleton. However, there might be differences in the local molecular organization of actin fibers, an idea supported by our TIRFm study and high-resolution Cav1 vesicle tracking analysis. Moreover, stress fibers appear to differ in FLNa-knockdown HeLa cells with respect to their control. A connection between Cav1 alignment or anchorage along actin stress fibers and inwards trafficking of Cav1 is supported by the results of FLNa- and FLNb-knockdown experiments, but the results obtained with the constitutively active mutant RhoAG14V suggest that increased Cav1 actin coalignment and/or anchorage does not always correlate with increased inwards trafficking. This might indicate that only physiological levels of RhoA activation allow optimal Cav1–actin anchorage, and that although anchorage is a prerequisite for inwards trafficking of Cav1, further increases do not correspond to an increase in internalization. Moreover, in the case of the non-phosphorylatable FLNa mutant, increased anchorage is accompanied by impaired inwards trafficking of Cav1. This finding, together with the results with the FLNa phosphomimetic mutant, suggests that FLNa phosphorylation at Ser2152 might regulate the anchorage of caveolae to the PM, and that cycling phosphorylation-dephosphorylation is required for inwards trafficking of caveolae. Expression of the constitutively active RhoA mutant, used to minimize any possible defect in stress fibers formation and distribution, did not restore the defect in Cav1 distribution upon FLNa depletion, suggesting that FLNa regulates Cav1 localization independently of its effect on stress fibers. However, we cannot rule out that active RhoA is not rescuing all potential actin differences between FLNa-depleted and control cells.

The high spatiotemporal resolution inherent to single-particle tracking in TIRFm indicated that, in the presence of FLNa, Cav1–GFP vesicles appear to become tightly bound, either as a result of direct interaction with FLNa or because FLNa promotes the build-up of specific vesicle-binding regions (anchoring points). In FLNa-depleted cells, although Cav1–GFP vesicles might become entangled near the basal PM, they do not seem to recognize a specific anchoring point. The effect of FLNa is not general for other actin crosslinking proteins because double-knockdown of α-actinin isoforms 1 and 4 did not affect these dynamics. The decrease in Cav1 anchoring after CytD or LatA treatment supports the notion that anchoring is mediated by the actin cytoskeleton. Moreover, the finding that RhoAG14V increases Cav1 anchorage only in the presence of FLNa further supports the idea that anchorage is facilitated by stress fiber stabilization and that FLNa is essential to mediate anchorage. The ability of FLNa to bind actin is also required for Cav1 anchoring because FLNa-shRNA^{R}-ABD is unable to restore the defect in HeLa-shFLNa. FLNa phosphorylation on Ser2152 seems to alter its link with the actin cytoskeleton, as suggested by the results obtained using the FLNa-shRNA^{R}-S2152A and the FLNa-shRNA^{R}-S2152E mutants. The non-phosphorylatable mutant increases anchorage events, whereas the phosphomimetic mutant is unable to restore anchoring. Neither of these extreme conditions is favorable for normal Cav1 function, and thus is not surprising that both affect its inwards trafficking.

Using TIRFm, a 41% decrease in the mobility of membrane-associated vesicles in cells with reduced FLNa over a comparatively long timescale of minutes has been reported previously (Sverdlov et al., 2009). However, using the same approach, we found no significant differences (supplementary material Fig. S4). This is consistent with the results from the high-resolution particle tracking, which showed no differences in the total mobility over this timescale; total displacement over 60 seconds was in the order of 500×500 nm, regardless of FLNa expression (data not shown). Significant differences between these two conditions were instead evident over short timescales; moreover, these differences did not relate to how much the Cav1–GFP vesicles moved, but to how they moved. Particle-tracking analysis and co-alignment studies of Cav1 and actin filaments suggest that FLNa anchors Cav1 vesicles at the PM by linking them to cortical actin. This role of FLNa could account for the association of caveolae with actin fibers, recently shown by Robert Parton's group; they identified a physical link between caveolae and actin fibers by an innovative and elegant EM technique (Richter et al., 2008). Our results suggest that FLNa is a strong candidate to be this physical linker.

To study caveolae internalization separately from the other patterns of caveolae trafficking, we stimulated inwards trafficking by de-adhesion of cells from the ECM (del Pozo et al., 2004). This approach thus provides an efficient tool for studying caveolae internalization, and moreover is physiologically relevant to polarized events, such as mitosis and directional cell migration, in which cells detach from the ECM in localized areas. For example, Cav1-mediated caveolae internalization at the cell rear regulates Rac1 PM targeting and hence directs cell migration (Grande-Garcia et al., 2007), and the absence of Cav1 internalization promotes cell proliferation and anchorage-independent growth (Cerezo et al., 2009). Our present results show that the compartment where Cav1 accumulates after de-adhesion colocalizes with Rab11, a marker of the REs (Sonnichsen et al., 2000). Distribution of Cav1 in a RE is consistent with its return to the PM after re-plating on fibronectin (del Pozo et al., 2005). Our results show that FLNa and FLNb are

both necessary for inwards trafficking of Cav1, suggesting that they might cooperate during this process. Evidence for a cooperative action between different isoforms has been described for caveolin itself (Cav1 and Cav2) in certain cell lines (Parton and Simons, 2007). In addition, some evidence has been also described for FLNa and FLNb, including co-expression in neurons and putative heterodimerization (Sheen et al., 2002). The role of filamins is specific, given that depletion of other actin crosslinkers such as α-actinin-1 and α-actinin-4 is dispensable for inwards trafficking of Cav1. Although we could not test the role of a FLNa mutant lacking the Cav1-binding sites due to poor protein expression and/or stability (data not shown), the fact that FLNa binds Cav1 (Stahlhut and van Deurs, 2000; Ravid et al., 2008) suggests that this association, in addition to FLNa–actin association, is important for Cav1 trafficking. The presence of FLNa in caveolae favors this idea (Stahlhut and van Deurs, 2000). The regulation of FLNa on inwards trafficking of Cav1 appears to be restricted to the first steps of this process. First, FLNa and Cav1 are both near the PM immediately after detachment, but dissociate after longer suspension periods. Second, FLNa regulates the distribution and anchorage of Cav1 along actin stress fibers, and actin regulates the first steps of Cav1 internalization (Parton et al., 1994; Echarri et al., 2007). Finally, early uptake of CTxB is delayed by FLNa depletion. The fact that CTxB uptake is not abolished might reflect the specificity of FLNa in caveolae internalization and the uptake of CTxB by other entry routes (Doherty and McMahon, 2009; Howes et al., 2010). A recent study concluded that FLNa regulates caveolae internalization in endothelial cells, on the basis of analysis of albumin uptake and transcytosis in the absence or presence of FLNa (Sverdlov et al., 2009). Collectively, this and the current study strongly suggest that caveolae internalization requires FLNa function. The decreased Cav1 internalization in FLNa-depleted cells, by increasing Rac1 signaling, stimulates the proliferation of adherent and suspended cells. The amount or distribution of the actin cytoskeleton in suspension is not altered by the absence of FLNa, despite the higher Rac1 signaling in this condition, probably because other factors required for actin polymerization are not be available during suspension. Moreover, alterations to cell migration in the absence of FLNa, which could be related to local distribution of Rac1, have been demonstrated (data not shown) (Xu et al., 2010).

We found that FLNa phosphorylation (Ser2152) is dynamically regulated during suspension, with an early increase (at 5 minutes) and a later decrease (at 60 minutes), and that these changes in phosphorylation are necessary for inwards trafficking of Cav1, given that neither of the Ser2152 mutants (non-phosphorylatable and phosphomimetic) was able to rescue defective inwards trafficking of Cav1 in FLNa-depleted cells. Phosphorylation on Ser2152 has been reported to regulate FLNa function (van der Flier and Sonnenberg, 2001). Ser2152 is not required for the binding of Cav1 to FLNa (Ravid et al., 2008), which supports our hypothesis that FLNa phosphorylation regulates the association with actin rather than with Cav1. Some studies report that phosphorylation of FLNa modulates its actin-binding capacity and actin crosslinking activity (Ohta and Hartwig, 1996; van der Flier and Sonnenberg, 2001; Wu et al., 1994; Zhuang et al., 1984), which might regulate the association of Cav1 with actin filaments. Our data suggest that PKC proteins, specifically PKCα, are involved in inwards trafficking of Cav1 probably through FLNa Ser2152 phosphorylation. However, the phosphorylation of FLNa in resting conditions is not heavily affected by PKC inhibitors, suggesting that this basal phosphorylation is mediated by other kinases (Ohta and Hartwig, 1995; Ravid et al., 2008; Vadlamudi et al., 2002; Woo et al., 2004).

Our data suggest a model (Fig. 7I) in which FLNa anchors caveolae at the PM by favoring a linkage with, and stop-and-go movement along, actin fibers. A certain level of Cav1 anchorage is required for its inwards trafficking upon cell detachment. In detached cells, a PKCα-dependent cycle of phosphorylation and dephosphorylation of FLNa at Ser2152 enables caveolae to separate from the PM and to internalize and accumulate in Rab11-positive REs. FLNa is thus a cofactor that links Cav1 and actin fibers; this association is required for proper organization of caveolae at the PM, and changes in this association upon FLNa phosphorylation are required for inwards trafficking of Cav1 vesicles.

Materials and Methods

Cell lines

293T/17 and HeLa cells were purchased from ATCC and were grown in Dulbecco's modified Eagle's medium (DMEM) supplemented with 10% fetal bovine serum (FBS) and 1% penicillin and streptomycin (and 4 μg/ml puromycin in shRNA-infected cells). M2 and A7 cells were kindly provided by Thomas P. Stossel (Brigham and Women's Hospital, Boston, MA) and Santos Mañes (Centro Nacional de Biotecnología, Madrid, Spain), and were grown in MEM supplemented with 10% FBS, 1% penicillin and streptomycin, 1% L-glutamine, 1 mg/l sodium pyruvate and 1 mg/l non-essential amino acids (and 500 ng/μl de G418 for A7 cells). HeLa cells expressing Cav1–GFP were kindly provided by Lukas Pelkmans (ETH, Zürich, Switzerland), and the GFP–Cav1 cells expressing low levels of GFP–Cav1 were selected by FACS (supplementary material Fig. S1K).

Reagents

siRNA oligonucleotide sequences were purchased from Dharmacon, Qiagen and Ambion. The 'all star control' (Qiagen) and 'on-target plus control' (Dharmacon) non-targeting siRNAs were used as controls (supplementary material Table S1).

Antibodies were sourced as follows. Polyclonal antibodies were against: caveolin (BD Transduction Laboratories), phosphorylated FLNa (Ser2152) (Cell Signaling), Dyn2 (Affinity Bio Reagents), Rab11 (Zymed Laboratories), pericentrin (Covance), PKCδ (Cell Signaling), phosphorylated histone 3 (Ser10) (Millipore), phosphorylated PAK (isoforms 1, 2 and 3) (Ser141) (Invitrogen), PAKα (Santa Cruz Biotechnology) and FLNb (Chemicon International). Monoclonal antibodies were against: FLNa (Chemicon International), α-tubulin, γ-tubulin and Flag M2 (Sigma), GFP (Roche), GM130, EEA1 and Cav2 (BD Transduction Laboratories), PKCα and α-actinin (recognizes isoforms 1 and 4) (Santa Cruz Biotechnology), RhoA and PKCε (Cell Signaling) and Rac1 (Millipore). Wheat germ agglutinin (WGA) was from Molecular Probes. CTxB, CytD and LatA were from Sigma-Aldrich.

Plasmids

pSMC2 vectors encoding FLNa or luciferase shRNAs and the pcDNA3 vector encoding FLNa WT shResistant dsRED (pcDNA3 FLNa-shRNA^R-WT-dsRED) were kindly provided by David A. Calderwood (Yale School of Medicine, New Haven, CT) (Baldassarre et al., 2009). To generate the plasmid encoding shRNA-resistant, non-phosphorylatable FLNa (FLNa-shRNA^R-S2152A-dsRED) and phosphomimetic FLNa (FLNa-shRNA^R-S2152E-dsRED) a PshAI-XbaI fragment from FLNa-shRNA^R-WT-dsRED was cloned into pGEMT easy, and the mutation was generated with the QuickChange II site-directed mutagenesis kit (Stratagene). The mutated fragments were then cloned into the PshAI-XbaI sites of the original vector. To generate the plasmid encoding shRNA-resistant FLNa with the actin-binding domain deleted (FLNa-shRNA^R-ABD-dsRED) a PshAI-PacI fragment excluding the actin-binding domain was amplified by PCR from an FLNa-pSCA intermediary vector. This fragment was then cloned into the PshAI-PacI sites of the original vector. The plasmid encoding Cav1–Flag was as described previously (del Pozo et al., 2005; Grande-Garcia et al., 2007). For the construction of MIGR1-Cav1-GFP, Cav1–GFP was amplified using primers containing PcII sites and then was subcloned into MIGR1 using the compatible NcoI sites. pEGFP RhoAG14V was as described previously (del Pozo et al., 1999). RhoAG14V was subcloned into pmCherry using BspEI and EcoRI sites. pCS2-memb-cherry, a construction containing two copies of the Lck membrane localizations signal, was kindly provided by Sean G. Megason (Harvard Medical School, Boston, MA). All sequences were confirmed by DNA sequencing.

Transfections and infections

Plasmid transfections were carried out with Fugene 6 (Roche). Transfections with siRNA oligonucleotides (30 or 100 nM) were performed with oligofectamine, as indicated by the manufacturer (Invitrogen). For retrovirus production, 293T/17 cells were transfected with retroviral vectors (Grande-Garcia et al., 2007).

Internalization assays and GM1 determination by FACS

De-adhesion-regulated internalization assays were as previously described (del Pozo et al., 2004). To stain GM1, live cells were treated at 4°C with 8 ng/ml of CTxB conjugated to Alexa Fluor 647, then fixed, washed and analyzed by FACS. The percentage of endocytosed GM1 was calculated from the ratio of surface CTxB staining at 60 and 0.25 minutes. To quantify CTxB intensity at the PM, a mask was created along both edges of the PM staining and the integrated intensity in the CTxB channel was measured using the measure RGB analyze plugin of Image J software.

Immunofluorescence microscopy

Cells were fixed at 4°C in 4% (w/v) paraformaldehyde (PFA) for 10 minutes, permeabilized with 0.2 % Triton X-100 for 5 minutes and blocked with 2% BSA for 1 hour. Images were taken with Leica TCS SP5 (confocal), Leica SPE (confocal) and Leica AM TIRF MC (TIRF) microscopes. TIRFm movies were acquired with a 100×1.46 NA oil-immersion objective, at 488 nm excitation and an evanescent field with a nominal penetration depth of 90 nm. Images were collected with an ANDOR iXon CCD at 85 ms per frame.

Visualizing inwards trafficking of Cav1–GFP in vivo

Cells were detached from the substratum using a mixture of trypsin and EDTA during a 70-minute period. The movie was acquired at 488 nm excitation with a Leica TCS SP5 confocal microscope fitted with a 63×1.4 NA oil-immersion objective. Images were acquired every 2 minutes.

Quantification of colocalization, inwards trafficking of Cav1 and length of the linear Cav1 pool

Colocalization of Cav1–GFP with intracellular compartment markers was quantified using the colocalization rate parameter in LAS AF software (Leica). Perinuclear distribution of Cav1 was quantified by measuring the perinuclear accumulation in the cell. A total of 150 cells per experiment were blindly quantified in at least three experiments. To calculate the total amount of the linear Cav1 pool, linearly organized immunostained Cav1 was identified and the length of the lines measured with the quantification module in Metamorph. The sum of the lengths of all identified Cav1 lines in control cells was assigned the value of 1, and the values obtained for the other conditions were expressed relative to this.

Cav1–GFP vesicle size and dynamic change analysis

For TIRFm movies, pictures were acquired every 300 ms. Cav1–GFP vesicles were quantified automatically using Cellprofiler software (Carpenter et al., 2006). To identify primary objects (Cav1–GFP vesicles), we limited the object size to a diameter of 1–9 pixels. We used an internal mix of Gaussian algorithms to threshold all images, assuming that 0.01% of the image was occupied by objects. A threshold correction factor of 1.4 was applied. To obtain the dynamic changes of Cav1 vesicles over long periods, we used the Delta-F-up ImageJ plugin to subtract the preceding image from the successive image in the stack. The *z*-projection over time of the subtracted stacks was created, and the signal-occupied area of the mask from the thresholded *z*-projection was calculated.

High spatiotemporal resolution particle tracking for Cav1–GFP

The lateral mobility of Cav1 vesicles near the basal PM of adherent cells was monitored by acquiring TIRFm image sequences and subsequent software-based vesicle tracking (Hellriegel et al., 2005). In each image, Cav1–GFP vesicles appeared as well-separated diffraction-limited spots of various intensities that were separated from each other by a few microns. This separation was sufficient to pinpoint the position of each vesicle with an accuracy of 20 to 50 nm, which is well below the optical resolution limit of ~300 nm. The center, amplitude and width of each pattern could thus be followed throughout the sequence. Some vesicles (10–15%) were excluded from the analysis, either because they rapidly disappeared from the observation plane or because they were in a crowded region, so that the obtained position could not be assigned unambiguously to a specific vesicle. In a typical experiment, we obtained ~30 Cav1–GFP vesicle trajectories per cell in a total of five cells for each of the six experiments. To quantify the anchoring behavior of these Cav1–GFP vesicles near the basal PM we defined an anchoring event as a situation in which the vesicle remains immobile to within the positioning accuracy (on average 30 nm) over a given timescale, chosen as follows. For timescales below 1 second the distinction between localized entanglement and a real anchoring event is less precise. For longer timescales (over 10 seconds) the Cav1–GFP vesicle motion becomes perturbed heavily by cell movement. Hence, we chose an intermediate timescale, in the order of 5 seconds (the number of frames varied depending on the acquisition time per frame, but was typically between 40 and 50 consecutive frames).

The individual trajectories of each tracked Cav1–GFP vesicle had a total length between 500 and 1000 frames. Each trajectory was analyzed by a software routine that scans through it in 50 frame segments. A positive anchoring event is counted if the segment stays within a circle of 30 nm radius over this interval. To avoid double-counting events that last for more than 50 frames, for example owing to a sporadic positioning spike or error, we introduced the condition that a new anchoring event must be separated from the previous one by at least five frames. From this analysis we obtained the total number of anchoring events in all trajectories, the total duration of each anchoring event, the total number of trajectories with at least one anchoring event and the total number of anchoring events per trajectory.

RNA extraction, reverse transcription and quantitative PCR

Total RNA was extracted using the Absolutely RNA system (Stratagene). cDNA was obtained by reverse transcription of 1 µg total RNA with random primers (Promega) and an Omniscript RT kit (Qiagen). For qPCR, 1 µl of each cDNA was used as template in a 20 µl qPCR reaction. qPCR reactions (repeated in triplicate) were carried out with the SYBR Green kit (Roche Diagnostics GmbH) and an ABI 7000 Sequence Detection System (Applied Biosystems). RNA from each sample was also included to ensure that no product was the result of genomic DNA contamination. PCR products were confirmed by dissociation curve analysis. Results were analyzed with qBase plus 1.1 software.

Statistical analysis

Mean values were compared using two-tailed paired Student's *t*-tests. Differences were considered as statistically significant at $P \leq 0.05$ and were labeled with asterisks ($*P \leq 0.05$; $**P \leq 0.01$; $***P \leq 0.005$).

We thank Thomas P. Stossel, Santos Mañes, Lukas Pelkmans, David A. Calderwood, Sean G. Megason and María Montoya for valuable reagents. We are grateful to Susana Minguet and Rubén Mota for help with FACS analysis and Juan Serrador for PKC antibodies and critical reading of the manuscript. Editorial assistance was provided by Simon Bartlett. O.M. was supported by a predoctoral fellowship from the Instituto de Salud Carlos III (Spanish Ministry of Science and Innovation, MICINN), A.E. by the Ramón y Cajal Program (MICINN), and L.B. by a predoctoral contract from the Comunidad Autónoma de Madrid. This work was supported by MICINN grants SAF2008-02100, Consolider CSD2009-00016 and RD06/0020/1033 ('Red Temática de Investigación Cooperativa en Cáncer' RTICC, Instituto de Salud Carlos III), by a EURYI (European Young Investigator) award from EUROHORCS (European Heads Of Research Councils) and the European Science Foundation (ESF), and by an EMBO Young Investigator Award, all to M.A.d.P. The CNIC is supported by the MICINN and the Pro-CNIC Foundation. O.M. designed and performed experiments, analyzed data and wrote the paper. M.A.d.P. conceived the project, designed experiments and wrote the paper. A.E. designed experiments and wrote the paper. C.H. performed single-vesicle tracking analysis. D.M.P. performed experiments and analyzed data. L.B. designed and constructed FLNa mutants along with O.M.

Supplementary material available online at
http://jcs.biologists.org/cgi/content/full/124/16/2763/DC1

References

Anderson, R. G. (1993). Caveolae: where incoming and outgoing messengers meet. *Proc. Natl. Acad. Sci. USA* **90**, 10909-10913.

Balasubramanian, N., Scott, D. W., Castle, J. D., Casanova, J. E. and Schwartz, M. A. (2007). Arf6 and microtubules in adhesion-dependent trafficking of lipid rafts. *Nat. Cell Biol.* **9**, 1381-1391.

Baldassarre, M., Razinia, Z., Burande, C. F., Lamsoul, I., Lutz, P. G. and Calderwood, D. A. (2009). Filamins regulate cell spreading and initiation of cell migration. *PLoS ONE* **4**, e7830.

Beekman, J. M., van der Poel, C. E., van der Linden, J. A., van den Berg, D. L., van den Berghe, P. V., van de Winkel, J. G. and Leusen, J. H. (2008). Filamin A stabilizes Fc gamma RI surface expression and prevents its lysosomal routing. *J. Immunol.* **180**, 3938-3945.

Bennett, J. P., Zaner, K. S. and Stossel, T. P. (1984). Isolation and some properties of macrophage alpha-actinin: evidence that it is not an actin gelling protein. *Biochemistry* **23**, 5081-5086.

Boucrot, E., Howes, M. T., Kirchhausen, T. and Parton, R. G. (2011). Redistribution of caveolae during mitosis. *J. Cell Sci.* **124**, 1965-1972.

Brotschi, E. A., Hartwig, J. H. and Stossel, T. P. (1978). The gelation of actin by actin-binding protein. *J. Biol. Chem.* **253**, 8988-8993.

Carpenter, A. E., Jones, T. R., Lamprecht, M. R., Clarke, C., Kang, I. H., Friman, O., Guertin, D. A., Chang, J. H., Lindquist, R. A., Moffat, J. et al. (2006). CellProfiler: image analysis software for identifying and quantifying cell phenotypes. *Genome Biol.* **7**, R100.

Cerezo, A., Guadamillas, M. C., Goetz, J. G., Sanchez-Perales, S., Klein, E., Assoian, R. K. and del Pozo, M. A. (2009). The absence of caveolin-1 increases proliferation and anchorage- independent growth by a Rac-dependent, Erk-independent mechanism. *Mol. Cell. Biol.* **29**, 5046-5059.

Chen, M. and Stracher, A. (1989). In situ phosphorylation of platelet actin-binding protein by cAMP-dependent protein kinase stabilizes it against proteolysis by calpain. *J. Biol. Chem.* **264**, 14282-14289.

Cox, D., Wessels, D., Soll, D. R., Hartwig, J. and Condeelis, J. (1996). Re-expression of ABP-120 rescues cytoskeletal, motility, and phagocytosis defects of ABP-120-Dictyostelium mutants. *Mol. Biol. Cell* **7**, 803-823.

Cunningham, C. C., Gorlin, J. B., Kwiatkowski, D. J., Hartwig, J. H., Janmey, P. A., Byers, H. R. and Stossel, T. P. (1992). Actin-binding protein requirement for cortical stability and efficient locomotion. *Science* **255**, 325-327.

del Pozo, M. A., Vicente-Manzanares, M., Tejedor, R., Serrador, J. M. and Sánchez-Madrid, F. (1999). Rho GTPases control migration and polarization of adhesion molecules and cytoskeletal ERM components in T lymphocytes. *Eur. J. Immunol.* **29**, 3609-3920.

del Pozo, M. A., Alderson, N. B., Kiosses, W. B., Chiang, H. H., Anderson, R. G. and Schwartz, M. A. (2004). Integrins regulate Rac targeting by internalization of membrane domains. *Science* **303**, 839-842.

del Pozo, M. A., Balasubramanian, N., Alderson, N. B., Kiosses, W. B., Grande-Garcia, A., Anderson, R. G. and Schwartz, M. A. (2005). Phospho-caveolin-1 mediates integrin-regulated membrane domain internalization. *Nat. Cell Biol.* **7**, 901-908.

Doherty, G. J. and McMahon, H. T. (2009). Mechanisms of endocytosis. *Annu. Rev. Biochem.* **78**, 857-902.

Echarri, A., Muriel, O. and Del Pozo, M. A. (2007). Intracellular trafficking of raft/caveolae domains: insights from integrin signaling. *Semin. Cell Dev. Biol.* **18**, 627-637.

Feng, Y., Chen, M. H., Moskowitz, I. P., Mendonza, A. M., Vidali, L., Nakamura, F., Kwiatkowski, D. J. and Walsh, C. A. (2006). Filamin A (FLNA) is required for cell-cell contact in vascular development and cardiac morphogenesis. *Proc. Natl. Acad. Sci. USA* **103**, 19836-19841.

Fernandez-Hernando, C., Yu, J., Suarez, Y., Rahner, C., Davalos, A., Lasuncion, M. A. and Sessa, W. C. (2009). Genetic evidence supporting a critical role of endothelial caveolin-1 during the progression of atherosclerosis. *Cell Metab.* **10**, 48-54.

Grande-Garcia, A., Echarri, A., de Rooij, J., Alderson, N. B., Waterman-Storer, C. M., Valdivielso, J. M. and del Pozo, M. A. (2007). Caveolin-1 regulates cell polarization and directional migration through Src kinase and Rho GTPases. *J. Cell Biol.* **177**, 683-694.

Hellriegel, C., Kirstein, J. and Brauchle, C. (2005). Tracking of single molecules as a powerful method to characterize diffusivity of organic species in mesoporous materials. *New J. Phys.* **7**, 23.

Howe, A. K. and Juliano, R. L. (2000). Regulation of anchorage-dependent signal transduction by protein kinase A and p21-activated kinase. *Nat. Cell Biol.* **2**, 593-600.

Howes, M. T., Kirkham, M., Riches, J., Cortese, K., Walser, P. J., Simpson, F., Hill, M. M., Jones, A., Lundmark, R., Lindsay, M. R. et al. (2010). Clathrin-independent carriers form a high capacity endocytic sorting system at the leading edge of migrating cells. *J. Cell Biol.* **190**, 675-691.

Isenberg, G. (1991). Actin binding proteins-lipid interactions. *J. Muscle Res. Cell Motil.* **12**, 136-144.

Isenberg, G. and Niggli, V. (1998). Interaction of cytoskeletal proteins with membrane lipids. *Int. Rev. Cytol.* **178**, 73-125.

Jay, D., Garcia, E. J. and de la Luz Ibarra, M. (2004). In situ determination of a PKA phosphorylation site in the C-terminal region of filamin. *Mol. Cell. Biochem.* **260**, 49-53.

Jimenez-Baranda, S., Gomez-Mouton, C., Rojas, A., Martinez-Prats, L., Mira, E., Ana Lacalle, R., Valencia, A., Dimitrov, D. S., Viola, A., Delgado, R. et al. (2007). Filamin-A regulates actin-dependent clustering of HIV receptors. *Nat. Cell Biol.* **9**, 838-846.

Kang, Y. S., Ko, Y. G. and Seo, J. S. (2000). Caveolin internalization by heat shock or hyperosmotic shock. *Exp. Cell Res.* **255**, 221-228.

Kanzaki, M. and Pessin, J. E. (2002). Caveolin-associated filamentous actin (Cav-actin) defines a novel F-actin structure in adipocytes. *J. Biol. Chem.* **277**, 25867-25869.

McMahon, K. A., Zajicek, H., Li, W. P., Peyton, M. J., Minna, J. D., Hernandez, V. J., Luby-Phelps, K. and Anderson, R. G. (2009). SRBC/cavin-3 is a caveolin adapter protein that regulates caveolae function. *EMBO J.* **28**, 1001-1015.

Megason, S. G. and Fraser, S. E. (2003). Digitizing life at the level of the cell: high-performance laser-scanning microscopy and image analysis for in toto imaging of development. *Mech. Dev.* **120**, 1407-1420.

Mundy, D. I., Machleidt, T., Ying, Y. S., Anderson, R. G. and Bloom, G. S. (2002). Dual control of caveolar membrane traffic by microtubules and the actin cytoskeleton. *J. Cell Sci.* **115**, 4327-4339.

Ohta, Y. and Hartwig, J. H. (1995). Actin filament cross-linking by chicken gizzard filamin is regulated by phosphorylation in vitro. *Biochemistry* **34**, 6745-6754.

Ohta, Y. and Hartwig, J. H. (1996). Phosphorylation of actin-binding protein 280 by growth factors is mediated by p90 ribosomal protein S6 kinase. *J. Biol. Chem.* **271**, 11858-11864.

Onoprishvili, I., Andria, M. L., Kramer, H. K., Ancevska-Taneva, N., Hiller, J. M. and Simon, E. J. (2003). Interaction between the mu opioid receptor and filamin A is involved in receptor regulation and trafficking. *Mol. Pharmacol.* **64**, 1092-1100.

Parrini, M. C., Camonis, J., Matsuda, M. and de Gunzburg, J. (2009). Dissecting activation of the PAK1 kinase at protrusions in living cells. *J. Biol. Chem.* **284**, 24133-24143.

Parton, R. G. (1994). Ultrastructural localization of gangliosides; GM1 is concentrated in caveolae. *J. Histochem. Cytochem.* **42**, 155-166.

Parton, R. G. and Simons, K. (2007). The multiple faces of caveolae. *Nat. Rev. Mol. Cell Biol.* **8**, 185-194.

Parton, R. G., Joggerst, B. and Simons, K. (1994). Regulated internalization of caveolae. *J. Cell Biol.* **127**, 1199-1215.

Pelkmans, L. and Zerial, M. (2005). Kinase-regulated quantal assemblies and kiss-and-run recycling of caveolae. *Nature* **436**, 128-133.

Pelkmans, L., Kartenbeck, J. and Helenius, A. (2001). Caveolar endocytosis of simian virus 40 reveals a new two-step vesicular-transport pathway to the ER. *Nat. Cell Biol.* **3**, 473-483.

Predescu, S. A., Predescu, D. N., Timblin, B. K., Stan, R. V. and Malik, A. B. (2003). Intersectin regulates fission and internalization of caveolae in endothelial cells. *Mol. Biol. Cell* **14**, 4997-5010.

Ravid, D., Chuderland, D., Landsman, L., Lavie, Y., Reich, R. and Liscovitch, M. (2008). Filamin A is a novel caveolin-1-dependent target in IGF-I-stimulated cancer cell migration. *Exp. Cell Res.* **314**, 2762-2773.

Richter, T., Floetenmeyer, M., Ferguson, C., Galea, J., Goh, J., Lindsay, M. R., Morgan, G. P., Marsh, B. J. and Parton, R. G. (2008). High-resolution 3D quantitative analysis of caveolar ultrastructure and caveola-cytoskeleton interactions. *Traffic* **9**, 893-909.

Rothberg, K. G., Heuser, J. E., Donzell, W. C., Ying, Y. S., Glenney, J. R. and Anderson, R. G. (1992). Caveolin, a protein component of caveolae membrane coats. *Cell* **68**, 673-682.

Seck, T., Baron, R. and Horne, W. C. (2003). Binding of filamin to the C-terminal tail of the calcitonin receptor controls recycling. *J. Biol. Chem.* **278**, 10408-10416.

Shajahan, A. N., Timblin, B. K., Sandoval, R., Tiruppathi, C., Malik, A. B. and Minshall, R. D. (2004). Role of Src-induced dynamin-2 phosphorylation in caveolae-mediated endocytosis in endothelial cells. *J. Biol. Chem.* **279**, 20392-20400.

Sharma, D. K., Brown, J. C., Choudhury, A., Peterson, T. E., Holicky, E., Marks, D. L., Simari, R., Parton, R. G. and Pagano, R. E. (2004). Selective stimulation of caveolar endocytosis by glycosphingolipids and cholesterol. *Mol. Biol. Cell* **15**, 3114-3122.

Sheen, V. L., Feng, Y., Graham, D., Takafuta, T., Shapiro, S. S. and Walsh, C. A. (2002). Filamin A and filamin B are co-expressed within neurons during periods of neuronal migration and can physically interact. *Hum. Mol. Genet.* **11**, 2845-2854.

Smart, E. J., Ying, Y. S. and Anderson, R. G. (1995). Hormonal regulation of caveolae internalization. *J. Cell Biol.* **131**, 929-938.

Sonnichsen, B., De Renzis, S., Nielsen, E., Rietdorf, J. and Zerial, M. (2000). Distinct membrane domains on endosomes in the recycling pathway visualized by multicolor imaging of Rab4, Rab5, and Rab11. *J. Cell Biol.* **149**, 901-914.

Stahlhut, M. and van Deurs, B. (2000). Identification of filamin as a novel ligand for caveolin-1: evidence for the organization of caveolin-1-associated membrane domains by the actin cytoskeleton. *Mol. Biol. Cell* **11**, 325-337.

Stossel, T. P., Condeelis, J., Cooley, L., Hartwig, J. H., Noegel, A., Schleicher, M. and Shapiro, S. S. (2001). Filamins as integrators of cell mechanics and signalling. *Nat. Rev. Mol. Cell Biol.* **2**, 138-145.

Sverdlov, M., Shinin, V., Place, A. T., Castellon, M. and Minshall, R. D. (2009). Filamin A regulates caveolae internalization and trafficking in endothelial cells. *Mol. Biol. Cell* **20**, 4531-4540.

Tagawa, A., Mezzacasa, A., Hayer, A., Longatti, A., Pelkmans, L. and Helenius, A. (2005). Assembly and trafficking of caveolar domains in the cell: caveolae as stable, cargo-triggered, vesicular transporters. *J. Cell Biol.* **170**, 769-779.

Thomsen, P., Roepstorff, K., Stahlhut, M. and van Deurs, B. (2002). Caveolae are highly immobile plasma membrane microdomains, which are not involved in constitutive endocytic trafficking. *Mol. Biol. Cell* **13**, 238-250.

Tigges, U., Koch, B., Wissing, J., Jockusch, B. M. and Ziegler, W. H. (2003). The F-actin cross-linking and focal adhesion protein filamin A is a ligand and in vivo substrate for protein kinase C alpha. *J. Biol. Chem.* **278**, 23561-23569.

Vadlamudi, R. K., Li, F., Adam, L., Nguyen, D., Ohta, Y., Stossel, T. P. and Kumar, R. (2002). Filamin is essential in actin cytoskeletal assembly mediated by p21-activated kinase 1. *Nat. Cell Biol.* **4**, 681-690.

van der Flier, A. and Sonnenberg, A. (2001). Structural and functional aspects of filamins. *Biochim. Biophys. Acta* **1538**, 99-117.

Woo, M. S., Ohta, Y., Rabinovitz, I., Stossel, T. P. and Blenis, J. (2004). Ribosomal S6 kinase (RSK) regulates phosphorylation of filamin A on an important regulatory site. *Mol. Cell. Biol.* **24**, 3025-3035.

Wu, M. P., Jay, D. and Stracher, A. (1994). Existence of multiple phosphorylated forms of human platelet actin binding protein. *Cell. Mol. Biol. Res.* **40**, 351-357.

Xu, Y., Bismar, T. A., Su, J., Xu, B., Kristiansen, G., Varga, Z., Teng, L., Ingber, D. E., Mammoto, A., Kumar, R. et al. (2010). Filamin A regulates focal adhesion disassembly and suppresses breast cancer cell migration and invasion. *J. Exp. Med.* **207**, 2421-2437.

Zhuang, Q. Q., Rosenberg, S., Lawrence, J. and Stracher, A. (1984). Role of actin binding protein phosphorylation in platelet cytoskeleton assembly. *Biochem. Biophys. Res. Commun.* **118**, 508-513.